Ceramics International 45 (2019) 510–515

Contents lists available at ScienceDirect

Ceramics International

journal homepage: www.elsevier.com/locate/ceramint

Two-step sintering behavior of titanium-doped Y_2O_3 ceramics with monodispersed sub-micrometer powder

Wook Ki Jung, Ho Jin Ma, Dong Gyu Kim, Do Kyung Kim*

Department of Materials Science and Engineering, Korea Advanced Institute of Science and Technology (KAIST), 291 Daehak-ro, Yuseong-gu, Daejeon 34141, Republic of Korea

ARTICLE INFO

Keywords:
Two-step sintering
Titanium-doped Y_2O_3
Kinetic window
Submicrometer powder
Sintering behavior

ABSTRACT

Two-step sintering of titanium-doped Y_2O_3 was carried out using monodispersed sub-micrometer powder. The effect of titanium dopant concentration on the sinterability and kinetic window of constant grain-size sintering were examined. The titanium doping improves the sinterability of the Y_2O_3 powder, which broadens the sintering kinetic window and lowers sintering temperature. The Vickers hardness was also enhanced as the doping concentration of titanium was increased, assuming the same grain size.

1. Introduction

Yttria (Y_2O_3) is considered one of the most suitable infrared window ceramics due to its long wavelength cutoff, high melting point, chemical stability, and low emissivity at high temperature [1–3]. With their unique properties, polycrystalline yttria ceramics have been fabricated with the development of ceramic processing and sintering technologies [4–16]. Researchers have been trying to improve the properties of yttria ceramics, but their poor mechanical properties impede their use in harsh environments. Tailoring the microstructure has been explored as a means of enhancing the mechanical properties of sintered yttria [17–21].

Two-step sintering, introduced by Chen and Wang, is an effective strategy to suppress grain growth during the final stage sintering and to obtain full density [22,23]. It induces triple point immobility (grain/pore junction) in a specific microstructure, thereby inhibiting grain growth during densification. The first step is reaching a higher temperature of T_1 to achieve high density and the next step is lowering the temperature to T_2 where it is maintained for a long time to achieve nearly full densification without further grain growth. The key condition for successful two-step sintering is obtaining a specific microstructure at T_1 with finer and uniform pore size distribution. Thereafter, the second step can have a temperature region, the so called 'kinetic window' that allows the production of fully densified ceramics with minimum grain growth.

Submicron-grained yttria ceramics have been fabricated by this two-step sintering technique. Transparent yttria ceramics were fabricated by using two-step sintering followed by a hot isostatic pressing (HIP) procedure [18]. They showed improved mechanical properties as a result of attaining full density with fine grains. Meanwhile, only a few dopants have been reported for two-step sintering of Y_2O_3. The effect of dopants such as Nb, Mg, Si, Er, Yb, Al, and Ti on mechanical strength were examined [24]. Among them, titanium-doped ceramics exhibited enhanced mechanical properties, but the effect of titanium doping on the two-step sintering behavior is not well understood and should be further studied.

The characteristics of the initial powder can also influence the two-step sintering behavior. The finer initial powder is advantageous for two-step sintering because there are more opportunities to achieve the critical density with finer microstructure. Many studies on two-step sintering have been conducted with ultrafine particles [25–27]. The finer particles are, however, easily agglomerated and the intra-agglomerated pores may become intragranular pores, which are difficult to eliminate even at high temperature sintering [28–30]. Considering this aspect, the importance of preparing a well-dispersed powder has been widely recognized over the past several decades [31–39]. A spherical powder with uniform and submicron size offers advantages in control of powder processing as well as reproducibility of the final products [40–43].

In the present work, two-step sintering behavior of titanium-doped yttria ceramics was investigated with monodispersed submicron powder. The effect of titanium doping concentration on sintering and grain growth was systematically evaluated. A small amount of titanium enhanced the grain boundary mobility in yttria, thus lowering the second-step temperature T_2. It was also found that the kinetic window becomes broader in titanium-doped yttria. The Vickers hardness was

* Corresponding author.
E-mail address: dkkim@kaist.ac.kr (D.K. Kim).

https://doi.org/10.1016/j.ceramint.2018.09.201
Received 6 August 2018; Received in revised form 10 August 2018; Accepted 19 September 2018
Available online 20 September 2018

improved with increasing titanium doping.

2. Experimental

Monodispersed spherical Y_2O_3 powder was synthesized by the homogeneous urea precipitation method. Commercial yttrium chloride hexahydrate ($YCl_3 \cdot 6H_2O$, 99.999%, Sigma-Aldrich) and urea (NH_2CONH_2, Sigma-Aldrich) were dissolved in distilled water to form a transparent solution. The concentration of Y^{3+} was kept at 0.02 M, while urea was kept at 1.5 M. The mixed solution was stirred and heated for 5 h at 85 °C. The resultant precursors were centrifuged and then washed seven times with distilled water and acetone to remove byproducts. The wet precipitate was dried, calcined at 1100 °C for 10 h, and homogeneously mixed with titanium oxide (TiO_2, rutile, > 99.98%, Sigma-Aldrich) by ball milling with ethanol for 24 h. The concentration of titanium doping was 0, 0.5, and 1 mol%, respectively.

All the prepared powders were dry-pressed under 20 MPa into a 15 mm diameter steel mold and subsequently were cold isostatically pressed under 200 MPa. The green compacts were sintered in a box furnace under an air atmosphere by conventional sintering and two-step sintering methods. The conventional sintering was carried out at 1300–1600 °C at a heating rate of 5 °C/min in 50 °C temperature intervals, and cooled naturally to room temperature. For the two step sintering, the green bodies were elevated to higher temperature (T_1) with a heating rate of 5 °C/min, and then cooled to lower temperature (T_2) with a cooling rate of 50 °C/min and held for 20 h.

The bulk density was measured by the Archimedes method using distilled water. All the ceramics were mirror-polished and thermally etched at 1100 °C for 20 min. The microstructure was observed using field emission scanning electron microscopy (FE-SEM Philips XL30FEG). At least 200 grains were measured for each ceramic to obtain the average grain size and distribution. Vickers hardness was measured using a Vickers hardness tester (VLPAK2000, Mitutoyo, Kawasaki, Japan) with a load of 1 kg on the specimen surface for 10 s. The hardness (H_v) was calculated by the following equation:

$$H_V = \frac{1.854P}{D^2} \quad (1)$$

where P is the applied load and D is the mean value of the diagonal length in the indentation prints.

3. Results and discussion

The as-calcined Y_2O_3 powder is shown in Fig. 1(a). It shows that a monodispersed spherical morphology was maintained even after the powder was calcined for a long time at high temperature. The measured average particle size and distribution is 206 ± 20 nm, as presented in Fig. 1(b). In this work, the small amount of titanium oxide was mixed with the calcined powder to prepare titanium-doped Y_2O_3 ceramics. The relative densities of green bodies were similar (55%) between the titania-mixed Y_2O_3 and undoped sample.

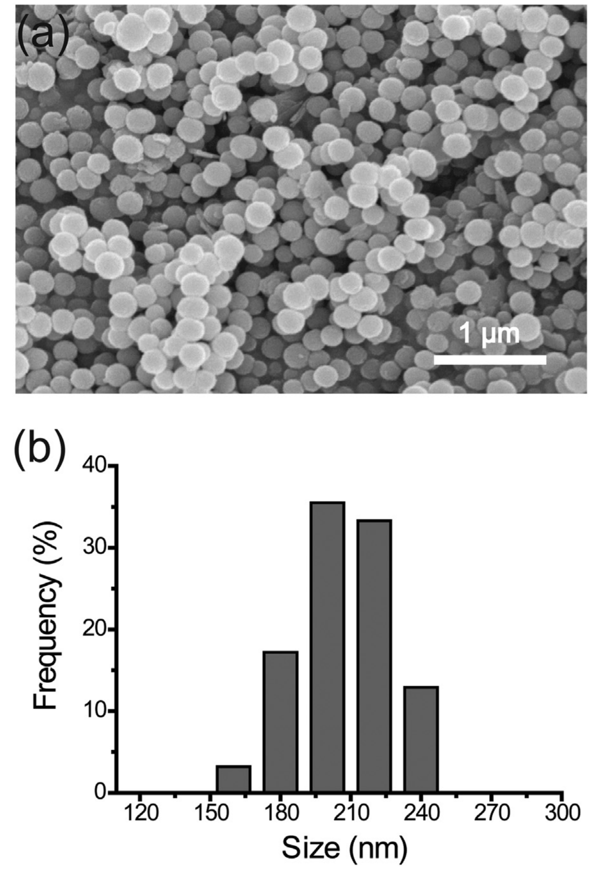

Fig. 1. (a) Morphology of monodispersed spherical Y_2O_3 powders calcined at 1100 °C for 10 h (b) Measured particle size distribution.

The relative density and grain size of sintered Y_2O_3 ceramics with different titanium doping concentration are shown in Fig. 2(a) and (b), respectively. Titanium-doped ceramics clearly show greater density and larger grain size compared to the undoped ceramics. With doping of titanium ions, the required sintering temperature to achieve a density above 97% is lowered by 150 °C. The relative density dramatically increases until 1450 °C with increasing doping concentration up to 1 mol %. At the same time, the grain size becomes twice the initial particle size at 1450 °C, which is equal to the grain size of pure yttria ceramics sintered at 1600 °C.

It was reported that titanium doping in Y_2O_3 enhanced the grain boundary mobility and also lowered the activation energy [44]. The yttrium interstitial defects are known to enhance the diffusion of Y_2O_3, and related defect chemistry indicates that divalent ion or tetravalent ion doping can produce yttrium interstitial or vacancy defects, respectively [45]. Tetravalent ions induce yttrium interstitial defects, resulting in enhanced grain growth. However, the exact mechanism underlying the titanium doping effect is unclear because the Ti^{4+} ions convert to a Ti^{3+} valence state during the sintering [17]. The grain boundary mobility enhancement may result from lattice distortion due to the differences in the ionic radius of the cations between titanium and yttrium ions. Further investigation is needed to understand the mechanism of grain boundary mobility enhancement in the titanium-doped yttria system.

The two-step sintering of Y_2O_3 monodispersed powders with different titanium doping concentration was conducted (Tables 1–3). According to Chen and Wang, the relative density of Y_2O_3 with critical microstructure at T_1 temperature is known to be above 75% to make pores unstable, allowing densification without grain growth. Moreover, the powder characteristics including particle size and morphology can remarkably influence the relative density at T_1 [46,47]. The sub-micrometer powders in this work exhibit the lowest density of 96% for the successful second step.

The kinetic windows for achieving full density without further grain growth are displayed in Fig. 3. The solid symbols indicate the G_1 and T_2 conditions to obtain only densification. The open symbols above the upper boundary line also showed full density but grain growth also occurred. The applied energy in the temperature during the second step is greater than the activation energy of grain boundary migration resulting in grain growth. The driving force for grain growth is decreased with increasing grain size. This is the reason why the upper boundary of kinetic window becomes higher as the grain size increases [22,23,46,48]. All of the arrows from the symbols reach the upper boundary line of the kinetic window. This means that average grain size is only one when the ceramics reach full density at the fixed T_2 temperature. The open symbols below the lower boundary line are

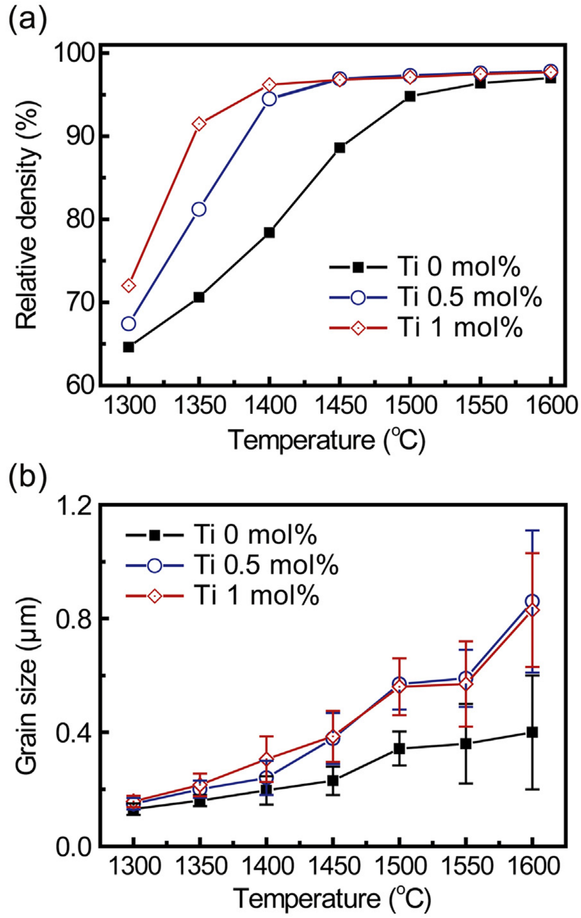

Fig. 2. The sintered Y_2O_3 ceramics with different Ti-doping concentration; (a) The relative density versus sintering temperature (b) Average grain size versus sintering temperature.

Table 1
Two-step sintering of Y_2O_3 ceramics with monodispersed spherical powder.

Samples	T_1(°C)	Relative density (%)	Grain size G_1 (μm)	T_2(°C)	Relative density (%)	Grain size G_2 (μm)
T0_TS1	1600	97.1	0.40	1375	99.6	0.41
T0_TS2	1550	96.4	0.36	1400	99.5	0.45
T0_TS3	1550	96.4	0.36	1375	99.5	0.37
T0_TS4	1550	96.4	0.36	1350	96.8	0.37
T0_TS5	1500	94.8	0.32	1450	98.8	0.58
T0_TS6	1500	94.8	0.32	1400	98.8	0.40
T0_TS7	1500	94.8	0.32	1350	94.8	0.32
T0_TS8	1450	88.5	0.23	1400	99.2	0.41
T0_TS9	1450	88.5	0.23	1350	88.5	0.30
T0_TS10	1450	88.5	0.23	1300	88.5	0.29

densification exhausted samples.

The kinetic window of the undoped yttria ceramics shows narrow width and is positioned at higher T_2 temperature compared with the titanium-doped products. On the other hand, the window of the titanium-doped samples shifts to a lower T_2 temperature region. The window shift to lower temperature indicates that the titanium doping enhances two-step sintering kinetics of yttria [24]. This titanium doping effect is consistent with the normal sintering results. The grain boundary mobility is greater in titanium-doped Y_2O_3, and it also enhances two step sintering kinetics, resulting in the T_2 temperature shift.

The window width of titanium-doped Y_2O_3 clearly is broadened with increasing grain size, G_1, compared to the undoped ceramics. This phenomenon is reported here for the first time and it indicates that for titanium-doped ceramics, larger grain size impedes grain boundary migration. The activation energy of titanium-doped Y_2O_3 is low enough to maintain the grain boundary mobility at lower temperature. It appears that the immobile triple points after the first step (T_1) become more remarkable in the case of titanium doping and larger grain size. This is advantageous for designing a two-step sintering strategy of monodispersed sub-micrometer Y_2O_3 powder.

Table 2
Two-step sintering of 0.5 mol% Ti-doped Y_2O_3 ceramics.

Samples	T_1(°C)	Relative density (%)	Grain size G_1 (μm)	T_2(°C)	Relative density (%)	Grain size G_2 (μm)
T0.5_TS1	1500	97.3	0.52	1450	99.6	1.12
T0.5_TS2	1500	97.3	0.52	1400	99.5	0.68
T0.5_TS3	1500	97.3	0.52	1350	99.2	0.52
T0.5_TS4	1500	97.3	0.52	1200	98.7	0.52
T0.5_TS5	1450	96.9	0.38	1400	99.0	0.72
T0.5_TS6	1450	96.9	0.38	1350	99.2	0.53
T0.5_TS7	1450	96.9	0.38	1300	99.0	0.38
T0.5_TS8	1450	96.9	0.38	1250	98.8	0.38
T0.5_TS9	1450	96.9	0.38	1200	97.5	0.38
T0.5_TS10	1400	81.2	0.20	1350	99.1	0.53
T0.5_TS11	1400	81.2	0.20	1250	95.9	0.25

Table 3
Two-step sintering of 1 mol% Ti-doped Y_2O_3 ceramics.

Samples	T_1(°C)	Relative density (%)	Grain size G_1 (μm)	T_2(°C)	Relative density (%)	Grain size G_2 (μm)
T1_TS1	1500	97.1	0.56	1450	99.9	0.77
T1_TS2	1500	97.1	0.56	1400	99.9	0.64
T1_TS3	1500	97.1	0.56	1350	99.9	0.58
T1_TS4	1450	96.8	0.39	1400	99.4	0.67
T1_TS5	1450	96.8	0.39	1350	99.5	0.55
T1_TS6	1450	96.8	0.39	1300	99.5	0.46
T1_TS7	1450	96.8	0.39	1250	99.5	0.39
T1_TS8	1450	96.8	0.39	1200	99.5	0.39
T1_TS9	1450	96.8	0.39	1150	98.0	0.39
T1_TS10	1400	91.5	0.21	1350	98.8	0.54
T1_TS11	1400	91.5	0.21	1250	98.7	0.34

The sintering paths of monodispersed sub-micrometer Y_2O_3 powders are summarized in Fig. 4. The average grain size increases with increasing relative density in the case of normal sintering. The pure Y_2O_3 has finer grain size and lower relative density even at high temperature, whereas the titanium-doped sample shows remarkable grain growth phenomenon. The normal sintering results were compared with the optimized two-step sintering paths in terms of achieving maximum density and minimum grain size (T0_TS3, T0.5_TS7, and T1_TS7). The grain size declined from 400 nm to 370 nm in the case of pure the Y_2O_3 ceramics denoted as T0_TS3. On the other hand, the grain size of Ti 1 mol% one (T1_TS7) shows a significant decrease from 830 nm to 390 nm. It is also emphasized that the minimum average grain size is similar (370 nm for undoped yttria and 390 nm for titanium-doped yttria) for the two-step sintered samples. These results indicate that suppression of grain growth via the two-step sintering method is more effective in titanium-doped Y_2O_3 ceramics.

The two-step sintered products with full density were measured for hardness. The Vickers hardness of the polycrystalline Y_2O_3 ceramics is strongly related to the average grain size, as described in Fig. 5. The variation in mechanical hardness with grain size follows the Hall-Petch behavior [49]. It is a dislocation pile up mechanism, which presents a linear relationship between the hardness value and the square root of the grain size. The ceramics with smaller grain size have a large number of grain boundaries that can act as obstacles to dislocation movement, thereby resulting in high hardness. Maximum hardness of 7.8 ± 0.1 GPa is achieved in the undoped Y_2O_3 with a grain size of 370 nm. The hardness of the Ti 1 mol% doped sample is improved to

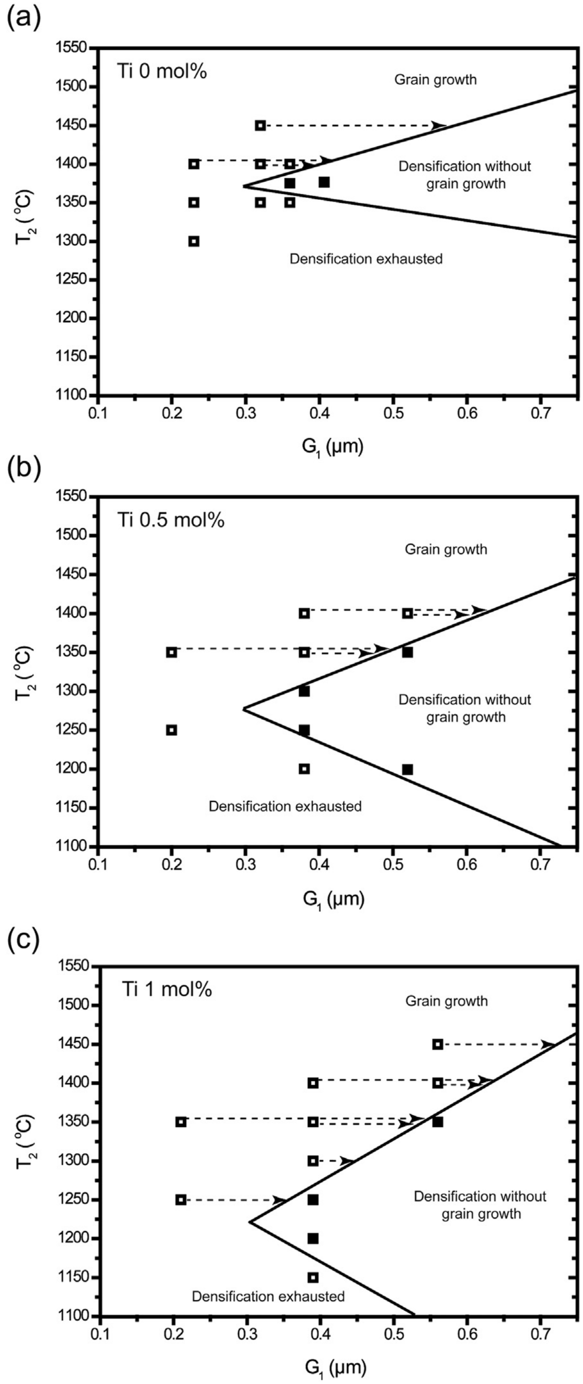

Fig. 3. Kinetic window for achieving full density without grain growth of monodispersed submicron Y_2O_3 powders; (a) Ti 0 mol% (b) Ti 0.5 mol% (c) Ti 1 mol%. Solid squares are reaching full densification without grain growth. Above the upper boundary line is grain growth with full densification, and below the lower line is densification exhausted.

8.4 ± 0.1 GPa with grain size of 390 nm. It is apparent that fully-densified Y_2O_3 ceramics have higher hardness values with increasing doping concentration, assuming the same grain size. The fracture of Y_2O_3 ceramics is mainly caused by grain boundaries, and mechanical properties can be improved by strengthening the grain boundaries. It was recognized that titanium ions preferentially locate in the grain boundaries and thereby strengthen these regions [17]. The enhanced hardness of titanium-ion doped Y_2O_3 is attributed to the grain boundary strengthening.

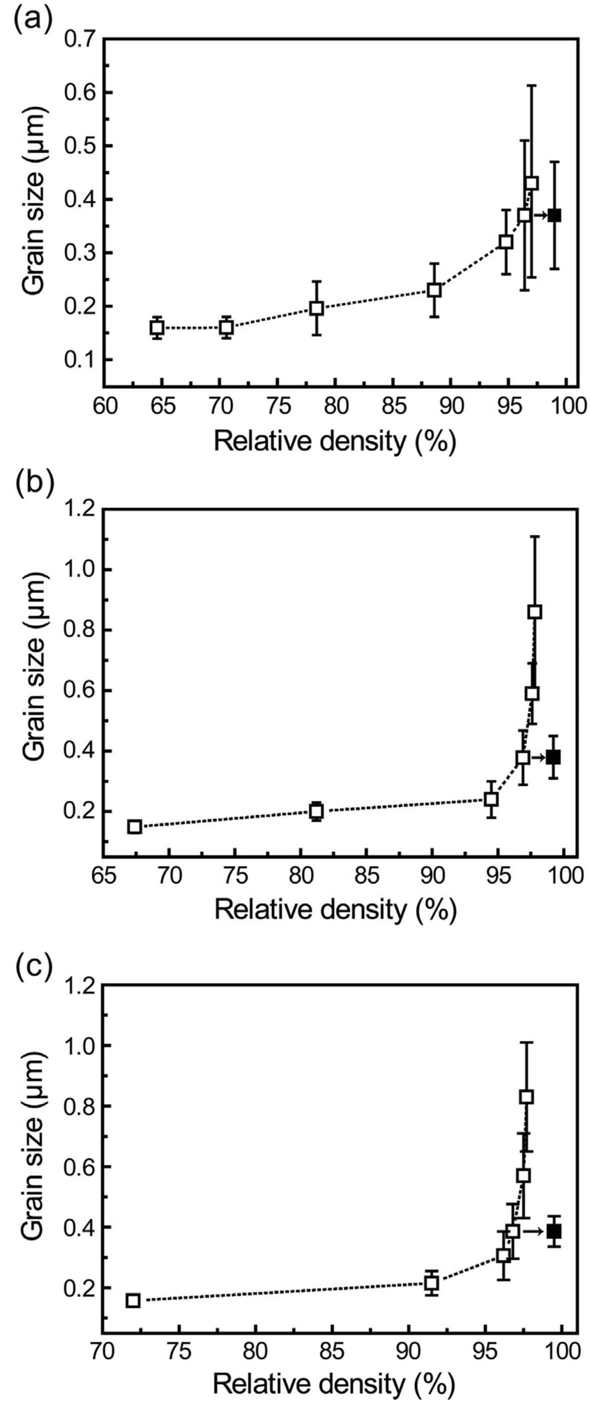

Fig. 4. Relative density and grain size curves of Y_2O_3 ceramics with different Ti-doping concentration in two-step sintering and conventional sintering; (a) Ti 0 mol% (b) Ti 0.5 mol%.

4. Conclusions

Titanium doping of Y_2O_3 sub-micrometer powder was conducted to investigate its effects on the two-step sintering behavior.

(1) The titanium dopant improves the sinterability of sub-micrometer Y_2O_3 powder by increasing the grain boundary mobility. Two-step sintering is more efficient in the case of titanium-doped Y_2O_3, enhancing densification and suppressing grain growth. The optimized grain size was 390 nm in the case of fully densified Ti 1 mol% Y_2O_3 ceramics starting from 206 ± 20 nm particle size.

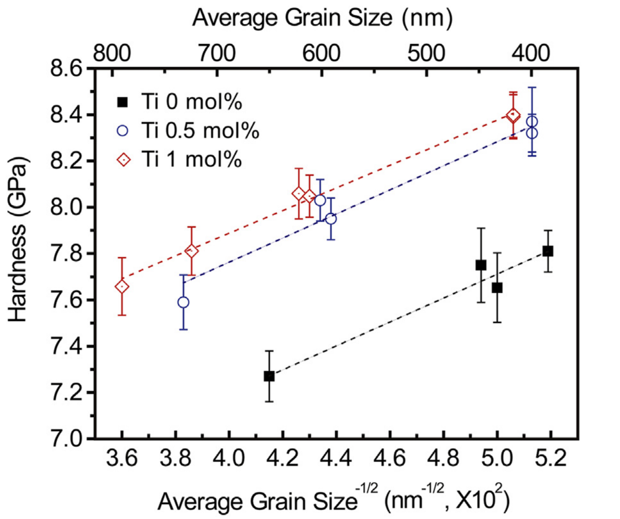

Fig. 5. Vickers hardness of two-step sintered Y_2O_3 ceramics with changing of the Ti doping concentration of 0, 0.5 and 1 mol%.

(2) The titanium dopant shifts the kinetic window to lower temperature (T_2) and significantly broaden the window width with increasing grain size (G_1) compared to pure Y_2O_3. This is advantageous for designing a two-step sintering strategy for sub-micrometer Y_2O_3 powders.

(3) The Vickers hardness increased from 7.8 to 8.4 GPa, depending on the titanium doping concentration. The titanium dopant enhanced the hardness of fully-densified Y_2O_3 ceramics, assuming the same grain size.

Acknowledgements

This work was supported by the Materials & Components Technology Development (MCTD) Program (Project no. 10047010) funded by the Ministry of Trade, Industry and Energy (MOTIE) of Korea.

References

[1] P. Hogan, T. Stefanik, C. Willingham, R. Gentilman, R. Integrated, D. Systems, Transparent Yttria for IR Windows and Domes – Past and Present (1) Initial Development of Transparent Yttrium Oxide The initial work in developing transparent yttrium oxide ceramics was carried out by General, 10^{th} DoD Electromagn. Wind. Symp, 2004.

[2] S.F. Wang, J. Zhang, D.W. Luo, F. Gu, D.Y. Tang, Z.L. Dong, G.E.B. Tan, W.X. Que, T.S. Zhang, S. Li, L.B. Kong, Transparent ceramics: processing, materials and applications, Prog. Solid State Chem. 41 (2013) 20–54.

[3] D.C. Harris, Durable 3–5 μm transmitting infrared window materials, Infrared Phys. Technol. 39 (1998) 185–201.

[4] L. Gan, Y.J. Park, H. Kim, J.M. Kim, J.W. Ko, J.W. Lee, Effects of pre-sintering and annealing on the optical transmittance of Zr-doped Y_2O_3 transparent ceramics fabricated by vacuum sintering conjugated with post-hot-isostatic pressing, Ceram. Int. 41 (2015) 9622–9627.

[5] L.L. Zhu, Y.J. Park, L. Gan, S. Il, Go, H.N. Kim, J.M. Kim, J.W. Ko, Q. Yi, S. Zhou, H. Teng, H. Lin, X. Hou, T. Jia, Effects of ZrO_2-La_2O_3 co-addition on the microstructural and optical properties of transparent Y_2O_3 ceramics, Ceram. Int. 43 (2017) 8525–8530.

[6] L. Gan, Y. Park, H. Kim, J. Kim, J. Ko, J. Lee, Fabrication and microstructure of hot pressed laminated Y_2O_3 /Nd:Y_2O_3/Y_2O_3 transparent ceramics, J. Eur. Ceram. Soc. Ceram. Soc. 36 (2016) 911–916.

[7] L. Gan, Y.-J. Park, M.-J. Park, H. Kim, J.-M. Kim, J.-W. Ko, J.-W. Lee, Facile fabrication of highly transparent yttria ceramics with fine microstructures by a hot-pressing method, J. Am. Ceram. Soc. 98 (2015) 2002–2004.

[8] D. Yan, X. Xu, H. Lu, Y. Wang, P. Liu, J. Zhang, Fabrication and properties of Y_2O_3 transparent ceramic by sintering aid combinations, Ceram. Int. 3 (2016) 5–8.

[9] W.K. Jung, H.J. Ma, Y. Park, D.K. Kim, A robust approach for highly transparent Y_2O_3 ceramics by stabilizing oxygen defects, Scr. Mater. 137 (2017) 1–4.

[10] W.K. Jung, H.J. Ma, S.W. Jung, D.K. Kim, Effects of calcination atmosphere on monodispersed spherical particles for highly optical transparent yttria ceramics, J. Am. Ceram. Soc. 100 (2017) 1876–1884.

[11] H.J. Ma, W.K. Jung, C. Baek, D.K. Kim, Influence of microstructure control on optical and mechanical properties of infrared transparent Y_2O_3-MgO nanocomposite, J. Eur. Ceram. Soc. 37 (2017) 4902–4911.

[12] Y. Huang, D. Jiang, J. Zhang, Q. Lin, Fabrication of transparent lanthanum-doped yttria ceramics by combination of two-step sintering and vacuum sintering, J. Am. Ceram. Soc. 92 (2009) 2883–2887.

[13] J. Zhang, L. An, M. Liu, S. Shimai, S. Wang, Sintering of Yb^{3+}:Y_2O_3 transparent ceramics in hydrogen atmosphere, J. Eur. Ceram. Soc. 29 (2009) 305–309.

[14] J. Zhang, S. Wang, L. An, M. Liu, L. Chen, Infrared to visible upconversion luminescence in Er^{3+}:Y_2O_3 transparent ceramics, J. Lumin. 122–123 (2007) 8–10.

[15] J. Wang, J. Zhang, D. Luo, H. Yang, D. Tang, L.B. Kong, Densification and microstructural evolution of yttria transparent ceramics: the effect of ball milling conditions, J. Eur. Ceram. Soc. 35 (2015) 1011–1019.

[16] J. Zhang, L. An, M. Liu, S. Shimai, S. Wang, Sintering of Yb^{3+}:Y_2O_3 transparent ceramics in hydrogen atmosphere, J. Eur. Ceram. Soc. 29 (2009) 305–309.

[17] H.R. Khosroshahi, H. Ikeda, K. Yamada, N. Saito, K. Kaneko, K. Hayashi, K. Nakashima, Effect of cation doping on mechanical properties of yttria prepared by an optimized two-step sintering process, J. Am. Ceram. Soc. 95 (2012) 3263–3269.

[18] K. Serivalsatit, B. Kokuoz, B. Yazgan-Kokuoz, M. Kennedy, J. Ballato, Synthesis, processing, and properties of submicrometer-grained highly transparent yttria ceramics, J. Am. Ceram. Soc. 93 (2010) 1320–1325.

[19] L. Zhang, Y. Ben, J. Wu, H. Yang, C. Wong, Q. Zhang, H. Chen, Alumina assisted grain refinement and physical performance enhancement of yttria transparent ceramics by two-step sintering, Mater. Sci. Eng. A 684 (2017) 466–469.

[20] L. Zhang, W. Pan, Structural and thermo-mechanical properties of Nd:Y_2O_3 transparent ceramics, J. Am. Ceram. Soc. 98 (2015) 3326–3331.

[21] K. Serivalsatit, B.Y. Kokuoz, B. Kokuoz, J. Ballato, Nanograined highly transparent yttria ceramics, Opt. Lett. 34 (2009) 1033–1035.

[22] X.H. Wang, P.L. Chen, I.W. Chen, Two-step sintering of ceramics with constant grain-size, I. Y_2O_3, J. Am. Ceram. Soc. 89 (2006) 431–437.

[23] X.H. Wang, P.L. Chen, I.W. Chen, Two-step sintering of ceramics with constant grain-size, II. $BaTiO_3$ and Ni-Cu-Zn ferrite, J. Am. Ceram. Soc. 89 (2006) 438–443.

[24] I.W. Chen, X.H. Wang, Sintering dense nanocrystalline ceramics without final-stage grain growth, Nature 404 (2000) 168–171.

[25] J. Nie, Y. Zhang, J.M. Chan, S. Jiang, R. Huang, J. Luo, Two-step flash sintering of ZnO: fast densification with suppressed grain growth, Scr. Mater. 141 (2017) 6–9.

[26] M. Mazaheri, A. Simchi, F. Golestani-Fard, Densification and grain growth of nanocrystalline 3Y-TZP during two-step sintering, J. Eur. Ceram. Soc. 28 (2008) 2933–2939.

[27] M. Mazaheri, A.M. Zahedi, S.K. Sadrnezhaad, Two-step sintering of nanocrystalline ZnO compacts: Effect of temperature on densification and grain growth, J. Am. Ceram. Soc. 91 (2008) 56–63.

[28] J.M. Kim, H.N. Kim, Y.J. Park, J.W. Ko, J.W. Lee, H.D. Kim, Fabrication of transparent $MgAl_2O_4$ spinel through homogenous green compaction by microfluidization and slip casting, Ceram. Int. 41 (2015) 13354–13360.

[29] L.C. Lim, P.M. Wong, M. Jan, Microstructural evolution during sintering of near-monosized agglomerate-free submicron alumina powder compacts, Acta Mater. 48 (2000) 2263–2275.

[30] X. Xu, X. Sun, H. Liu, J.G. Li, X. Li, D. Huo, S. Liu, Synthesis of monodispersed spherical yttrium aluminum garnet (YAG) powders by a homogeneous precipitation method, J. Am. Ceram. Soc. 95 (2012) 3821–3826.

[31] Y. Li, Y. Wu, Transparent and luminescent ZnS ceramics consolidated by vacuum hot pressing method, J. Am. Ceram. Soc. 98 (2015) 2972–2975.

[32] N. Saito, S. Matsuda, T. Ikegami, Fabrication of transparent yttria ceramics at low temperature using carbonate-derived powder, J. Am. Ceram. Soc. 81 (1998) 2023–2028.

[33] H. Choi, S. Yong, D.K. Kim, Synthesis and compaction behavior of monodispersed 3Y-ZrO_2 spherical agglomerates, J. Korean Ceram. Soc. 50 (2013) 434–438.

[34] T. Ikegami, J. Li, T. Mori, Y. Moriyoshi, Fabrication of transparent yttria ceramics by the low-temperature synthesis of yttrium hydroxide, J. Am. Ceram. Soc. 85 (2002) 1725–1729.

[35] Churl Hee Cho, Do Kyung Kim, D.H. Kim, Photocatalytic activity of monodispersed spherical TiO_2 particles with different crystallization routes, J. Am. Ceram. Soc. 86 (2003) 1138–1145.

[36] B.-K. Lee, Y.-H. Jung, D.-K. Kim, Synthesis of monodisperse spherical SiO_2 and self-assembly for photonic crystals, J. Korean Ceram. Soc. 46 (2009) 472–477.

[37] H.K. Park, D.K. Kim, C.H. Kim, Thermal hydrolysis of $TiCl_4$, J. Am. Ceram. Soc. 80 (1997) 743–749.

[38] J.Y. Choi, C.H. Kim, D.K. Kim, Hydrothermal synthesis of spherical perovskite oxide powders using spherical gel powders, J. Am. Ceram. Soc. 81 (1998) 1353–1356.

[39] D. Sordelet, M. Akinc, Preparation of spherical, monosized Y_2O_3 precursor particles, J. Colloid Interface Sci. 122 (1988) 47–59.

[40] Y. Huang, D. Jiang, J. Zhang, Q. Lin, Z. Huang, Synthesis of mono-dispersed spherical Nd:Y_2O_3 powder for transparent ceramics, Ceram. Int. 37 (2011) 3523–3529.

[41] D. Sordelet, M. Akinc, Sintering of monosized, spherical yttria powders, J. Am. Ceram. Soc. 71 (1988) 1148–1153.

[42] J. He, X. Li, S. Liu, Q. Zhu, J.-G. Li, X. Sun, Effects of pre-treatment of starting powder with sulfuric acid on the fabrication of yttria transparent ceramics, J. Eur. Ceram. Soc. 35 (2015) 2369–2377.

[43] J.J. Shan, C.H. Li, J.M. Wu, J.A. Liu, A.N. Chen, Y.S. Shi, Sintering behavior and microstructural evolution of the monodispersed β-gallium oxide micro-particles with different morphology and size, Ceram. Int. 43 (2017) 16843–16850.

[44] M. Kodo, K. Soga, H. Yoshida, T. Yamamoto, Doping effect of divalent cations on sintering of polycrystalline yttria, J. Eur. Ceram. Soc. 30 (2010) 2741–2747.

[45] P. Chen, I. Chen, Grain boundary mobility in Y_2O_3: defect mechanism and dopant

effects, J. Am. Ceram. Soc. 79 (1996) 1801–1809.
[46] K. Serivalsatit, J. Ballato, Submicrometer grain-sized transparent erbium-doped scandia ceramics, J. Am. Ceram. Soc. 93 (2010) 3657–3662.
[47] K. Bodišová, P. Šajgalík, D. Galusek, P. Švančárek, Two-stage sintering of alumina with submicrometer grain size, J. Am. Ceram. Soc. 90 (2007) 330–332.
[48] X.H. Wang, X.Y. Deng, H. Zhou, L.T. Li, I.W. Chen, Bulk dense nanocrystalline $BaTiO_3$ ceramics prepared by novel pressureless two-step sintering method, J. Electroceram. 21 (2008) 230–233.
[49] I.J. McColm, Ceramic Hardness, Springer Science & Business Media, 2013.